Chapter 9

Numerically and Analytically Forecasting the Coal Burst Using Energy Based Approach Methods

Faham Tahmasebinia, Chengguo Zhang,
Ismet Canbulat, Onur Vardar and Serkan Saydam

Additional information is available at the end of the chapter

http://dx.doi.org/10.5772/intechopen.71879

Abstract

Coal burst is referred to as the violent failure of overstressed coal, which has been recognised as one of the most critical dynamic failures in coal mines. This chapter aims to analytically and numerically evaluate the energy transformation between the different strata and coal layers. An accurate closed-form solution is developed. Due to the complexity of the causes and mechanisms contributing to the coal burst occurrence, 3D finite element modelling as well as discrete element models will be developed to validate the suggested analytical assessments of rock/coal burst occurrence. The energy concept is emphasised in order to improve the understanding of the underlying mechanisms of coal burst. Only with enhanced understanding of the driving mechanisms, a reliable coal burst risk assessment can be achieved.

Keywords: analytical modelling, numerical modelling, released energy, coal burst, failure mechanism

1. Introduction

One of the critical engineering problems faced by the coal mining industry is coal burst. It is caused by a dynamic release of energy within the overstressed rock mass/coal during the mining process. It occurs under the effects of complex environments of geology, stress and mining conditions. It has been recognised that the unstable releases of potential energy of the rock around the excavations, mainly in the form of kinetic energy, contributes to the coal burst occurrence. Interactions between the coal and rock interface, as well as the confinement, can completely determine the failure mode and the ultimate bearing capacity of coal pillars, influencing the amount of stored energy within a pillar. Many authors define rock/coal burst

INTECH
open science | open minds

© 2018 The Author(s). Licensee InTech. This chapter is distributed under the terms of the Creative Commons Attribution License (http://creativecommons.org/licenses/by/3.0), which permits unrestricted use, distribution, and reproduction in any medium, provided the original work is properly cited. CC BY

as a sudden, rapid rupture of the rock mass with a violent, explosive release of elastic/strain energy from the surface of an excavation, which is generally associated with a seismic event and produces rock particle ejections [1–5]. The coal burst source is the mechanism that triggers or induces the damage mechanism visible on the excavation surface. The coal burst source is generally associated with a seismic event that can be performed at a wide range of local magnitudes, normally ranging from undetectable up to 5 [6]. Indeed, mining-induced seismicity can reach moderate values of ground velocity and acceleration, and in some cases its effects on the surface can be compared with low-intensity earthquakes [7]. The mechanism that produces the seismic event is a sudden release of the strain energy that has been stored above a critical level within the rock/coal mass. Some portion of this energy is demolished by crack development, and the rest of the energy is converted into the kinetic energy [8, 9]. When the energy source is located near the roadway, the released energy may lead to coal fragmentation. At the place of the source of the energy, where it is located in a plane of weakness inside the coal mass, the released energy provokes shear displacement along the plane, which in revolve generate vibrations that persuade coal ejections when they are situated near the excavation boundaries [7]. Tarasov and Randolph [6] have explained a number of special and inconsistent behaviours of hard rock at the significant depth that are directly related to rock failure mechanisms in deep excavations. They determined that the procedures of the shear failure, with respect to the significant low friction, can be classified as the main reason to release energy. Based on the suggested frictionless mechanism, the level of the brittleness of the confined rock/coal masses might be increased under high stress conditions. This may result in reducing the overall ductility which would in line with the abrupt fracture failure. Under an energy-balance approach, the methods to predict coal burst risk are based on energy indexes such as energy release rate (ERR) [8–10], energy storage rate (ESR), strain energy storage index (WET) [11], potential energy of elastic strain (PES) or strain energy density (SED) (i.e., the elastic strain energy in a unit volume of the coal mass, which can be computed by the uni-axial compressive strength of the coal and the relevant unloading tangential modulus), and burst potential index (BPI). A combination of both analytical as well as numerical methods, where they can comprehensively evaluate the structural performance of the mine scale, would be broadly addressed in the current research. Thus, the following aims explicitly will be addressed.

1. Develop a full 2D and 3D finite element as well as discrete element models to compute the inducted energies in a single pillar with different high to width ratios. In this approach, different loading conditions varying from the static, quasi-static as well as dynamic loading will be exclusively examined.

2. Considering the effect of the energy transformations between the rock/coal layers due to the different contact/joint properties.

3. Suggest empirical equations to predict the amount of the released strain energy due to the mining activities.

The main novelty of this research is to simulate the effect of the failure and post-failure of the engaged material as well as joint/contact properties on the energy transformation.

http://dx.doi.org/10.5772/intechopen.71879

2. Numerical modelling strategy

Numerical simulations can be considered as an individual tool to predict possible failure modes and the actual capacity of the mining setting. It is mostly useful to undertake parametric and sensitivity analyses to gain better understanding the nature and level of indecision, or remaining hazard, associated with design process.

First, a finite element model is developed by taking advantage from the commercial software package ABAQUS/Explicit. All the geotechnical components, including the rock and coal, were modelled by the eight-node linear brick element (C3D8R) available in the ABAQUS library. Element C3D8R relies on reducing integration and hourglass control. The assigned meshes were established by using the structured technique available in ABAQUS. The solution to the nonlinear problem was sought using the explicit dynamic analysis procedure available in ABAQUS. In the current study, **Figure 1** presents a quarter of a single pillar.

Thus, by taking advantage from the symmetrical boundary conditions, a finer mesh was assigned to the model. Finding the right input material properties would be a significant assumption, which has not been appropriately studied in the available literature. Modelling of mechanical behaviour of the coal under both compression and shear stresses would be very complicated, since there are no articulated reports which might be concerned with the uni-axial and tri-axial behaviour of coal under both static and dynamic loading conditions. According to

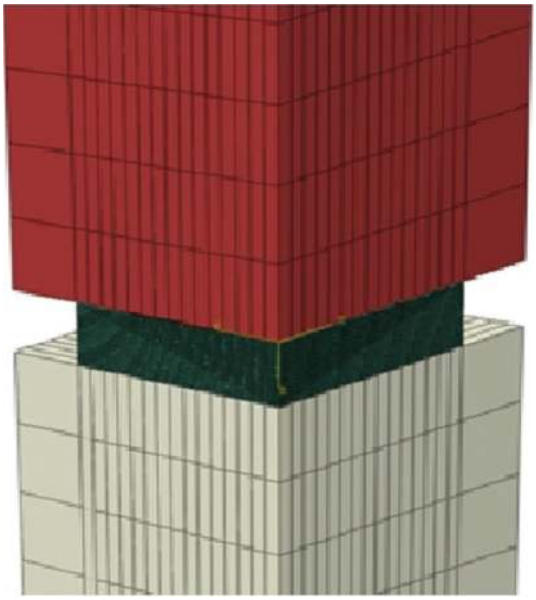

Figure 1. Illustration of a typical single pillar model using ABAQUS/Explicit.

the elastic analysis, the stress analysis and energy computations were organised in line with the linear relationship between the stress and the strain in coal and overburden properties. The peak and post-peak behaviour of coal and surrounding rock masses will be ignored. Therefore, in the current literature, the computed stress, strain and kinetic energy have been noticeably overestimated. At the second stage, a combination of the 2D and 3D discrete element models using UDEC and 3DEC was developed. **Figure 2** illustrates the pillar model incorporating half of coal, roof and floor along the symmetrical centre-line of the pillar. The height of the roof and floor was 20 m and the mining height was fixed at 3 m, while the pillar widths varied in order to simulate the pillars with width to height (w/h) ratios from 1 to 5.

A Mohr-Coulomb (MC) material that presents a constant strength after failure and a Mohr-Coulomb strain-softening material that can reach the peak strength and then decrease to a residual strength have been considered. A quasi-static loading condition as a velocity was applied on the top and bottom of the model. The applied velocity was started with a very small, constant velocity to represent a relative loading system to promote a model of a coal failure that progresses slowly. Simulating a proper loading/displacement condition is significantly crucial, specifically, gaining a sound understanding of the structural reaction of a single

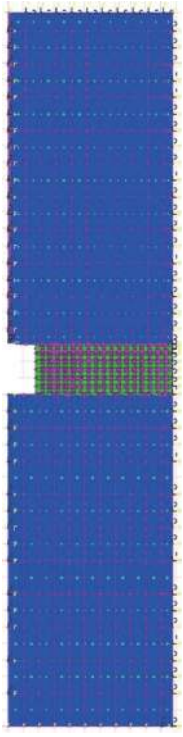

Figure 2. Geometry and zoning of coal pillar model using UDEC.

http://dx.doi.org/10.5772/intechopen.71879

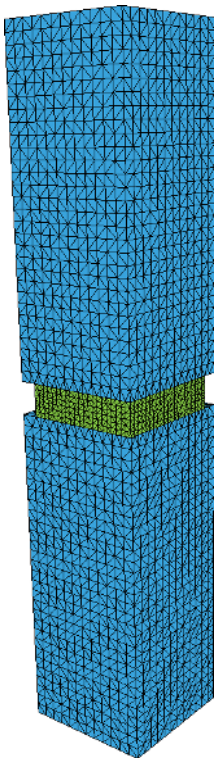

Figure 3. Geometry and zoning of coal pillar model using 3DEC.

coal sample under dynamic or quasi-static loading conditions. Consideration was also given to defining a joint interface. A Coulomb Slip (CS) joint interface property, where it is represented by displacement softening parameters, was taken into account to simulate the interface properties between the different joints.

The uniform zone size of 0.1 m was applied to the coal, and a smooth variation of zoning from the coal to the boundaries was used for roof and floor with appropriate aspect ratios to avoid numerical instability. Roller boundaries were applied along the side of the roof and floor, the bottom of the floor and the vertical line. The same trend was applied to develop the three-dimensional discrete element using 3DEC (see **Figure 3**).

3. Analytical approach

An analytical method is developed to evaluate shear stress and strain distributions between the engaged surfaces throughout different joint layers by considering the beam theory

method in different directions with respect to the different planes, where it can independently calculate shear forces between the different layers and shear strain as well as the curvature distribution along the different layers that have been extracted. The main concept to derive the following equations was extracted from [12, 13]. The cross-sectional analysis is based on the assumption of the Euler-Bernoulli beam model. The strain distribution across the section can be calculated by $\varepsilon = \varepsilon_r - y \times \kappa$, where ε_r is the strain at the reference point (which can be determined at any point), y is the distance between the selected point and location of the neutral axis of the cross-section and κ is the curvature across the section in different strata layers. A vector can be introduced by $K(D)$ which will be included in the internal action N (axial forces) and M (internal moment). External loads, which might be due to the effect of the self-weight of the strata layers as well as the possible applied forces due to the vertical or horizontal displacement in the different layers, can induce the external axial force N_e and external moment M_e. The relationship between the internal and external actions can be presented by:

$$\varepsilon = \begin{bmatrix} \varepsilon_r \\ \kappa \end{bmatrix} \tag{1}$$

$$r(\varepsilon) = \begin{bmatrix} N \\ M \end{bmatrix} \tag{2}$$

$$r_e = \begin{bmatrix} N_e \\ M_e \end{bmatrix} \tag{3}$$

$$r(\varepsilon) = r_e \quad \text{(This is the vector for strain)} \tag{4}$$

By considering the nonlinear interactions, the presented equations can be re-written by:

$$r\left(\varepsilon^{(i+1)}\right) = r\left(\varepsilon^{(i)}\right) + r_t\left(\varepsilon^{(i)}\right) \times \Delta\varepsilon^{(i)} = r_e \tag{5}$$

$$r_t\left(\varepsilon^{(i)}\right) \times \Delta\varepsilon^{(i)} = r_R^{(i)} \tag{6}$$

$$r_R^{(i)} = r_e - r\left(\varepsilon^{(i)}\right) \tag{7}$$

$$\frac{\partial N\left(\varepsilon_r^{(i)}, \kappa^{(i)}\right)}{\partial \varepsilon_r} \times \Delta\varepsilon_r^{(i)} + \frac{\partial N\left(\varepsilon_r^{(i)}, \kappa^{(i)}\right)}{\partial \kappa} \times \Delta\kappa = N_R^{(i)} \tag{8}$$

$$N_R^{(i)} = N_e - N\left(\varepsilon_r^{(i)}, \kappa^{(i)}\right) \tag{9}$$

$$M_R^{(i)} = M_e - M\left(\varepsilon_r^{(i)}, \kappa^{(i)}\right) \tag{10}$$

All the equations can be re-presented in matrix format:

$$r_t\left(\varepsilon^{(i)}\right) = \begin{bmatrix} \dfrac{\partial N\left(\varepsilon_r^{(i)}, \kappa^{(i)}\right)}{\partial \varepsilon_r} & \dfrac{\partial N\left(\varepsilon_r^{(i)}, \kappa^{(i)}\right)}{\partial \kappa} \\ \dfrac{\partial M\left(\varepsilon_r^{(i)}, \kappa^{(i)}\right)}{\partial \varepsilon_r} & \dfrac{\partial M\left(\varepsilon_r^{(i)}, \kappa^{(i)}\right)}{\partial \kappa} \end{bmatrix} \tag{11}$$

$$\Delta\varepsilon^{(i)} = \begin{bmatrix} \Delta\varepsilon_r^{(i)} \\ \Delta\kappa^{(i)} \end{bmatrix} \quad \text{(Changing strain and curvature)} \tag{12}$$

$$r_R^{(i)} = \begin{bmatrix} N_R^{(i)} \\ M_R^{(i)} \end{bmatrix} \tag{13}$$

The partial derivatives of N and M with respect to ε_r and κ can be re-arranged in a more practical form, recalling the definitions of internal actions as:

$$\frac{\partial N\left(\varepsilon_r^{(i)}, \kappa^{(i)}\right)}{\partial \varepsilon_r} = \int \frac{\partial \sigma}{\partial \varepsilon_r} dA \tag{14}$$

$$\frac{\partial N\left(\varepsilon_r^{(i)}, \kappa^{(i)}\right)}{\partial \kappa} = \int \frac{\partial \sigma}{\partial \kappa} dA \tag{15}$$

$$\frac{\partial M\left(\varepsilon_r^{(i)}, \kappa^{(i)}\right)}{\partial \varepsilon_r} = -\int y \frac{\partial \sigma}{\partial \varepsilon_r} dA \tag{16}$$

$$\frac{\partial M\left(\varepsilon_r^{(i)}, \kappa^{(i)}\right)}{\partial \kappa} = -\int y \frac{\partial \sigma}{\partial \kappa} dA \tag{17}$$

where the values of the stress depend on the constitutive models adopted for the materials and on the magnitude of the strain

$$\frac{\partial N\left(\varepsilon_r^{(i)}, \kappa^{(i)}\right)}{\partial \varepsilon_r} = \int \frac{\partial \sigma}{\partial \varepsilon_r} dA = \int \frac{\partial \sigma}{\partial \varepsilon} \times \frac{\partial \varepsilon}{\partial \varepsilon_r} dA = \int \frac{\partial \sigma}{\partial \varepsilon} \times \frac{\partial (\varepsilon_r - y \times \kappa)}{\partial \varepsilon_r} dA = \int \frac{\partial \sigma}{\partial \varepsilon} dA \tag{18}$$

$$\frac{\partial N\left(\varepsilon_r^{(i)}, \kappa^{(i)}\right)}{\partial \kappa} = \int \frac{\partial \sigma}{\partial \kappa} dA = \int \frac{\partial \sigma}{\partial \varepsilon} \times \frac{\partial (\varepsilon_r - y \times \kappa)}{\partial \kappa} dA = -\int y \times \frac{\partial \sigma}{\partial \varepsilon} dA \tag{19}$$

$$\frac{\partial M\left(\varepsilon_r^{(i)}, \kappa^{(i)}\right)}{\partial \varepsilon_r} = -\int y \times \frac{\partial \sigma}{\partial \varepsilon_r} dA = -\int y \times \frac{\partial \sigma}{\partial \varepsilon} \times \frac{\partial (\varepsilon_r - y \times \kappa)}{\partial \varepsilon_r} dA = -\int y \times \frac{\partial \sigma}{\partial \varepsilon} dA \tag{20}$$

$$\frac{\partial M\left(\varepsilon_r^{(i)}, \kappa^{(i)}\right)}{\partial \kappa} = -\int y \times \frac{\partial \sigma}{\partial \varepsilon_r} dA = -\int y \times \frac{\partial \sigma}{\partial \varepsilon} \times \frac{\partial (\varepsilon_r - y \times \kappa)}{\partial \kappa} dA = \int y^2 \times \frac{\partial \sigma}{\partial \varepsilon} dA \tag{21}$$

$$\sigma = E \times \varepsilon \quad \text{for} \quad |\varepsilon| \le \varepsilon_p \ \text{(elastic strain)} \tag{22}$$

$$\sigma = f_p \quad \text{for} \quad |\varepsilon| > \varepsilon_p \ \text{(plastic strain)} \tag{23}$$

$$\frac{\partial \sigma}{\partial \varepsilon} = \frac{\partial (E \times \varepsilon)}{\partial \varepsilon} = E \quad \text{for} \quad |\varepsilon| \le \varepsilon_p \ \text{(elastic strain)} \tag{24}$$

$$\frac{\partial \sigma}{\partial \varepsilon} = \frac{\partial \left(f_p\right)}{\partial \varepsilon} = 0 \quad \text{for} \quad |\varepsilon| > \varepsilon_p \ \text{(plastic strain)} \tag{25}$$

$$N\left(\varepsilon_r^{(i)}, \kappa^{(i)}\right) = \int \sigma dA = \sum_{j=1}^{n_j} \sigma\left(y_j, \varepsilon_r^{(i)}, \kappa^{(i)}\right) \times A_j \tag{26}$$

$$M\left(\varepsilon_r^{(i)}, \kappa^{(i)}\right) = -\int y\sigma dA = -\sum_{j=1}^{n_j} y_j \times \sigma\left(y_j, \varepsilon_r^{(i)}, \kappa^{(i)}\right) \times A_j \tag{27}$$

$$\frac{\partial N\left(\varepsilon_r^{(i)}, \kappa^{(i)}\right)}{\partial \varepsilon_r} = \int \frac{\partial \sigma}{\partial \varepsilon} dA = \sum_{j=1}^{n_j} \frac{\partial \sigma\left(y_j, \varepsilon_r^{(i)}, \kappa^{(i)}\right)}{\partial \varepsilon} \times A_j \tag{28}$$

$$\frac{\partial N\left(\varepsilon_r^{(i)}, \kappa^{(i)}\right)}{\partial \kappa} = -\int y \times \frac{\partial \sigma}{\partial \varepsilon_r} dA = -\sum_{j=1}^{n_j} y_j \times \frac{\partial \sigma\left(y_j, \varepsilon_r^{(i)}, \kappa^{(i)}\right)}{\partial \varepsilon} \times A_j \tag{29}$$

$$\frac{\partial M\left(\varepsilon_r^{(i)}, \kappa^{(i)}\right)}{\partial \varepsilon_r} = -\int y \times \frac{\partial \sigma}{\partial \varepsilon_r} dA = -\sum_{j=1}^{n_j} y_j \times \frac{\partial \sigma\left(y_j, \varepsilon_r^{(i)}, \kappa^{(i)}\right)}{\partial \varepsilon} \times A_j \tag{30}$$

$$\frac{\partial M\left(\varepsilon_r^{(i)}, \kappa^{(i)}\right)}{\partial \kappa} = \int y^2 \times \frac{\partial \sigma}{\partial \varepsilon} dA = \sum_{j=1}^{n_j} y_j^2 \times \frac{\partial \sigma\left(y_j, \varepsilon_r^{(i)}, \kappa^{(i)}\right)}{\partial \varepsilon} \times A_j \tag{31}$$

$$\mathrm{r}\,(\mathrm{x}, \mathrm{d_e}) = \begin{bmatrix} \mathrm{N}(\mathrm{x}, \mathrm{d_e}) \\ \mathrm{M}(\mathrm{x}, \mathrm{d_e}) \end{bmatrix} = \begin{bmatrix} \int_{\mathrm{A}} \sigma(\mathrm{x}, \mathrm{y}, \mathrm{d_e}) \mathrm{dA} \\ -\int_{\mathrm{A}} \mathrm{y}\sigma(\mathrm{x}, \mathrm{y}, \mathrm{d_e}) \mathrm{dA} \end{bmatrix} = \begin{bmatrix} \sum_{j=1}^{n_j} \sigma(\mathrm{x}, \mathrm{y}, \mathrm{d_e}) \mathrm{A_j} \\ -\sum_{j=1}^{n_j} \mathrm{y_j} \sigma(\mathrm{x}, \mathrm{y}, \mathrm{d_e}) \mathrm{A_j} \end{bmatrix} \tag{32}$$

$$I = \int_a^b f(x)dx = \left(\frac{b-a}{2}\right) \times \int_{-1}^{1} f\left(\frac{a+b}{2} + \frac{b-a}{2} \times \overline{x}\right) = \left(\frac{b-a}{2}\right) \times \sum_{k=1}^{n_G} w_k \times f\left(\frac{a+b}{2} + \frac{b-a}{2} \times \overline{x_k}\right) \tag{33}$$

$$\mathrm{k_e}(x, \mathrm{d_e}) = \int_L \mathrm{B^T}(x) \mathrm{r}(\mathrm{x}, \mathrm{d_e})\, \mathrm{dx} = \frac{\mathrm{L}}{2} \sum_{\mathrm{k}=1}^{n_\mathrm{G}} w_k \mathrm{B^T}(x_k) \mathrm{r}(x_k, \mathrm{d_e}) \tag{34}$$

$$\mathrm{q_e} = \int_L \mathrm{N_e^T(x)p(x)dx} = \frac{\mathrm{L}}{2}\sum_{\mathrm{k=1}}^{n_G} w_k \mathrm{N_e^T}(x_k)p(x_k) \quad x_k = \frac{\mathrm{L}}{2}(\overline{x_k}+1) \tag{35}$$

$$\begin{bmatrix} u(x) \\ v(x) \end{bmatrix} = \begin{bmatrix} N_{u1}(x) & 0 & 0 & N_{u2}(x) & N_{u3}(x) & 0 & 0 \\ 0 & N_{v1}(x) & N_{v2}(x) & 0 & 0 & N_{v3}(x) & N_{v4}(x) \end{bmatrix} \times \begin{bmatrix} u_L \\ v_L \\ \theta_L \\ u_M \\ u_R \\ v_R \\ \theta_R \end{bmatrix} = \mathrm{N_e(x)d_e} \tag{36}$$

$$N_{u1}(x) = 1 - \frac{3x}{L} + \frac{2x^2}{L^2} \tag{37}$$

$$N_{u2}(x) = \frac{4x}{L} + \frac{4x^2}{L^2} \tag{38}$$

$$N_{u3}(x) = -\frac{x}{L} + \frac{2x^2}{L^2} \tag{39}$$

$$N_{v1}(x) = 1 - \frac{3x^2}{L^2} + \frac{2x^2}{L^3} \tag{40}$$

$$N_{v2}(x) = x - \frac{2x^2}{L} + \frac{x^3}{L^2} \tag{41}$$

$$N_{v3}(x) = \frac{3x^2}{L^2} - \frac{2x^3}{L^3} \tag{42}$$

$$N_{v4}(x) = -\frac{x^2}{L} + \frac{x^3}{L^2} \tag{43}$$

$$\begin{aligned} u(x) &= N_{u1}(x)u_L + N_{u2}(x)u_M + N_{u3}(x)u_R \\ v(x) &= N_{v1}(x)v_L + N_{v2}(x)\theta_L + N_{v3}(x)v_R + N_{v4}(x)\theta_R \end{aligned} \tag{44}$$

$$B(x) = \begin{bmatrix} N'_{u1}(x) & 0 & 0 & N'_{u2}(x) & N'_{u3}(x) & 0 & 0 \\ 0 & N''_{v1}(x) & N''_{v2}(x) & 0 & 0 & N''_{v3}(x) & N''_{v4}(x) \end{bmatrix} \tag{45}$$

$$N'_{u1}(x) = -\frac{3}{L} + \frac{4x}{L^2} \tag{46}$$

$$N'_{u2}(x) = \frac{4}{L} - \frac{8x}{L^2} \tag{47}$$

$$N'_{u3}(x) = -\frac{1}{L} + \frac{4x}{L^2} \tag{48}$$

$$N''_{v1}(x) = \frac{12x}{L^3} - \frac{6}{L^2} \tag{49}$$

$$N''_{v2}(x) = \frac{6x}{L^2} - \frac{4}{L} \tag{50}$$

$$N''_{v3}(x) = \frac{6}{L^2} - \frac{12x}{L^3} \tag{51}$$

$$N''_{v4}(x) = \frac{6x}{L^2} - \frac{2}{L} \tag{52}$$

$$\mathrm{k_e}\left(x, \mathrm{d_e^{(i)}}\right) = \frac{\mathrm{L}}{2} \sum_{\mathrm{k}=1}^{n_\mathrm{G}} w_k \mathrm{B^T}(x_k) \mathrm{r^{(i)}}\left(x_k, \mathrm{d_e^{(i)}}\right) = \frac{\mathrm{L}}{2} \sum_{\mathrm{k}=1}^{n_\mathrm{G}} w_k \times \begin{bmatrix} N'_{u1}(x_k) & 0 \\ 0 & N''_{v1}(x_k) \\ 0 & N''_{v2}(x_k) \\ N'_{u2}(x_k) & 0 \\ N'_{u3}(x_k) & 0 \\ 0 & N''_{v3}(x_k) \\ 0 & N''_{v4}(x_k) \end{bmatrix} \times \begin{bmatrix} \mathrm{N}\left(x_k, \mathrm{d_e^{(i)}}\right) \\ \mathrm{M}\left(x_k, \mathrm{d_e^{(i)}}\right) \end{bmatrix} \tag{53}$$

$$\mathrm{q_e} = \frac{\mathrm{L}}{2} \sum_{\mathrm{k}=1}^{n_\mathrm{G}} w_k \times \begin{bmatrix} N_{u1}(x_k) & 0 \\ 0 & N_{v1}(x_k) \\ 0 & N_{v2}(x_k) \\ N_{u2}(x_k) & 0 \\ N_{u3}(x_k) & 0 \\ 0 & N_{v3}(x_k) \\ 0 & N_{v4}(x_k) \end{bmatrix} \times \begin{bmatrix} n(x_k) \\ w(x_k) \end{bmatrix} \tag{54}$$

$$\mathrm{N}\left(x_k, \mathrm{d_e^{(i)}}\right) = \sum_{j=1}^{n_j} \sigma\left(\mathrm{x_k}, \mathrm{y_i}, \mathrm{d_e^{(i)}}\right) \mathrm{A_j} \tag{55}$$

$$\mathrm{M}\left(x_k, \mathrm{d_e^{(i)}}\right) = -\sum_{j=1}^{n_j} \mathrm{y_j} \sigma\left(\mathrm{x_k}, \mathrm{y_i}, \mathrm{d_e^{(i)}}\right) \mathrm{A_j} \tag{56}$$

Thus, by calculating stress and strain at the different points in the different layers of the overburden, the internal axial forces as well as internal moments can be calculated. It was assumed that the strain energy can be calculated by:

http://dx.doi.org/10.5772/intechopen.71879

$$A = \frac{1}{2} \times \iiint \left(\sigma_{xx} \times \varepsilon_{xx} + \sigma_{yy} \times \varepsilon_{yy} + \sigma_{zz} \times \varepsilon_{zz} + \sigma_{xy} \times \varepsilon_{xy} + \sigma_{xz} \times \varepsilon_{xz} + \sigma_{yz} \times \varepsilon_{yz}\right) dxdydz \quad (57)$$

where $\sigma_{xx} \times \varepsilon_{xx}$, ……, $\sigma_{yz} \times \varepsilon_{yz}$ can be calculated, according to the principal of the virtual work and virtual deformation $\delta A = \delta R_1 + \delta R_2$, when the induced stresses and strains cannot be directly extracted from the simulated model.

4. Energy calculation based on the numerical approach

According to Xie et al. [14], the coal burst proneness of a coal can be determined by the coal burst proneness assessments. Special attentions were devoted by the number of researchers to develop coal burst proneness indexes, which are broadly utilised, such as elastic energy, impact energy, dynamic failure time as well as elastic deformation and stiffness ratio indexes. The elastic energy index WET is defined as the ratio of the elastic strain energy and the strain energy dissipation at point E (75–85% of the peak strength). As shown in **Figure 4**, the ratio of the area SEAC (between the unloaded line EA and the strain axis) and the area SEOA (between the load and unload line) is the elastic energy index

$$W_{ET} = \left(\frac{S_{EAC}}{S_{EOA}}\right) \quad (58)$$

The impact energy index KE is defined as the ratio of the pre-peak area and the post-peak area, KE namely, the ratio of energy in the pre-peak stage and the energy released in the post-peak stage.

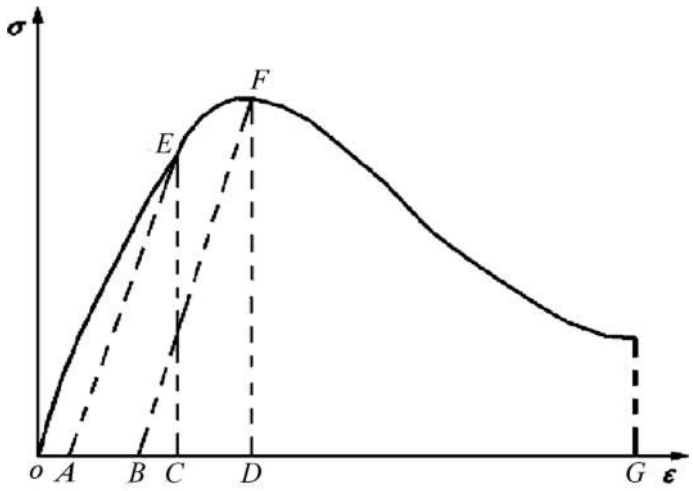

Figure 4. A typical stress-strain curve.

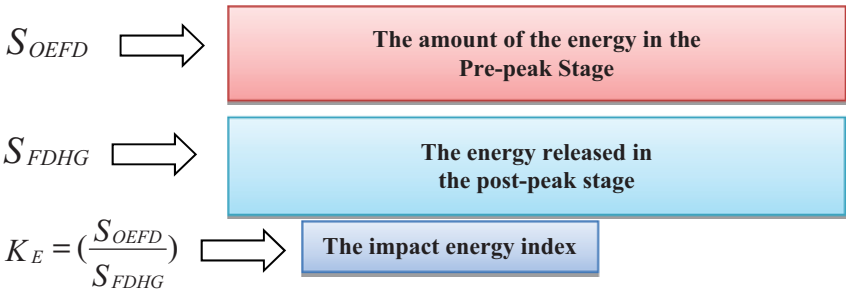

5. Energy calculation based on the analytical approach

According to Xie et al. [14], dissipated and released energy can play a significant role which may result in coal deformation and failure. Based on the failure mechanism, the fracture procedure of a coal mass might be started from a partial fracture which would be followed by local damage. This procedure will be finally resulting in collapsing the mining structures. The failure process is thermodynamically permanent, which includes released and dissipated energy. The dissipated energy can cause damage as well as a permanent deformation of the coal mass, which is followed by weakening of strength. A sudden release of the strain energy may lead to a catastrophic failure, which clearly indicates a certain condition where the coal mass collapses. The released and dissipated energy from the coal mass, individually, plays an essential role in the relevant sudden failure, which would be one of the major requirements to investigate the procedure of the deformation and failure of a coal mass. **Figure 5** is a typical compression curve of coal under a constant displacement.

Figure 5 explicitly demonstrates the calculation of the dissipated, released and residual energies. With respect to the constant development of the inner micro-defects, energy dissipation is an indispensable characteristic of the deformation and failure of the coal mass. The evolution declines the strength of the coal, which may result in total failure. In this content, the dissipated energy is directly concerned with the damage as well as mitigating strength of the coal.

$$u_{d1} = \int_0^{\varepsilon_1} (\sigma_a d\varepsilon) = \sum_0^{\varepsilon_1} \left[\left(\varepsilon_{1(i)} - \varepsilon_{1(i-1)} \right) \times \left(\frac{\sigma_{a(i)} + \sigma_{a(i-1)}}{4} \right) \right] \quad \text{Dissipated energy before peak} \quad (59)$$

$$u_{d2} = \int_{\varepsilon_3}^{\varepsilon_4} (\sigma_c d\varepsilon) = \sum_{\varepsilon_3}^{\varepsilon_4} \left[\left(\varepsilon_{(j)} - \varepsilon_{(j-1)} \right) \times \left(\frac{\sigma_{c(j)} + \sigma_{c(j-1)}}{4} \right) \right] \quad \text{Dissipated energy after peak} \quad (60)$$

$$u_r = \int_{\varepsilon_1}^{\varepsilon_2} (\sigma_m d\varepsilon) = \sum_{\varepsilon_1}^{\varepsilon_2} \left[\left(\varepsilon_{(k)} - \varepsilon_{(k-1)} \right) \times \left(\frac{\sigma_{m(k)} + \sigma_{m(k-1)}}{4} \right) \right] \quad \text{Released elastic energy} \quad (61)$$

$$u_{ed} = \int_{\varepsilon_2}^{\varepsilon_3} \left(\sigma_p d\varepsilon\right) = \sum_{\varepsilon_2}^{\varepsilon_3} \left[\left(\varepsilon_{(l)} - \varepsilon_{(l-1)}\right) \times \left(\frac{\sigma_{p(l)} + \sigma_{p(l-1)}}{4} \right) \right] \quad \text{Residual elastic energy} \tag{62}$$

Tables 1 and **2** presents a comparison between the different elastic and post-failure energy components using UDEC and 3DEC output results as well as semi-close form solutions. As it can be found, there is a good agreement between the suggested semi-analytical methods as well as the calculated key energy components which were extracted from the UDEC and 3DEC output results.

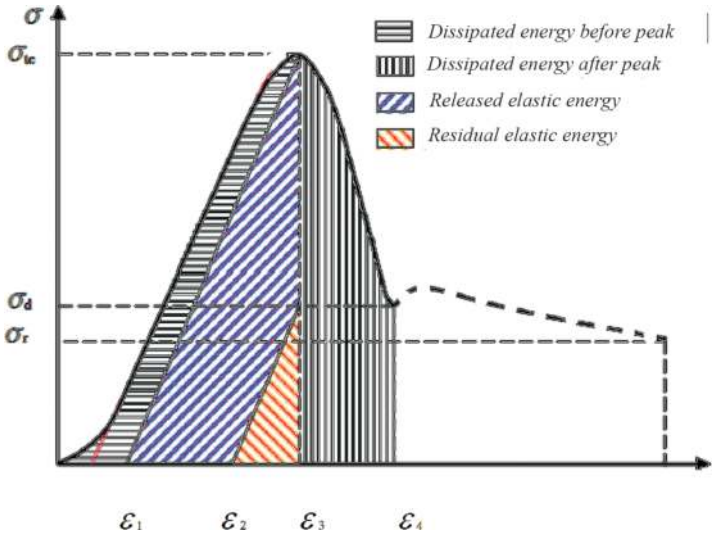

Figure 5. Analytically calculation of dissipated energy and released energy (Xie et al. [14]).

	Elastic strain energy (kJ/m^3)		Dissipated elastic strain energy (kJ/m^3)		The amount of the energy in the pre-peak stage (kJ/m^3)		The energy released in the post-peak stage (kJ/m^3)	
Ratio (w/h)	**UDEC**	**Analytic**	**UDEC**	**Analytic**	**UDEC**	**Analytic**	**UDEC**	**Analytic**
1	1.56	1.63	0.78	0.77	3.61	3.73	12.47	10.59
1.5	1.92	1.35	0.8	0.78	7.89	7.44	12.48	11.03
2	2.0621	2.004	0.991	0.92	10.22	9.83	18.31	17.09
2.5	4.70	4.82	1.16	1.11	14.47	13.43	21.17	23.14
3	11.13	10.58	2.51	2.41	35.825	32.87	11.73	10.6
4	14.72	13.27	4.07	4.60	60.26	55.00	56.34	70.02
5	16.63	16.24	5.334	5.37	75.83	73.67	91.19	84.04

Table 1. A comparison between the different energy components (UDEC and the analytical solution).

	Elastic strain energy (kJ/m^3)		Dissipated elastic strain energy (kJ/m^3)		The amount of the energy in the pre-peak stage (kJ/m^3)		The energy released in the post-peak stage (kJ/m^3)	
Ratio (w/h)	**3DEC**	**Analytic**	**3DEC**	**Analytic**	**3DEC**	**Analytic**	**3DEC**	**Analytic**
1	2.58	2.65	1.767	1.55	4.91	4.77	14.87	14.77
1.5	2.94	2.37	1.88	0.78	8.88	8.46	16.56	15.23
2	4.24	4.01	2.891	2.92	12.55	11.98	21.23	20.14
2.5	6.72	6.84	3.18	3.11	15.37	15.41	24.35	23.99
3	13.15	12.62	5.51	5.44	37.15	36.87	28.45	27.68
4	16.76	16.27	7.07	7.20	60.26	62.33	59.11	57.88
5	19.83	19.28	8.334	8.22	76.22	75.12	96.54	92.66

Table 2. A comparison between the different energy components (3DEC and the analytical solution).

6. Progress of the failure in different pillar ratios

Different loading conditions varying from the quasi-static to dynamic loading has been applied to the coal pillar with the different width to height (w/h) ratio to determine the pillar capability as well as the possible observed failure modes. A strain-based criterion, as a major failure criterion, was implemented in the ABAQUS/Explicit to predict of the cracking path due to the different applied loadings as well as different pillar geometrical properties. A quarter

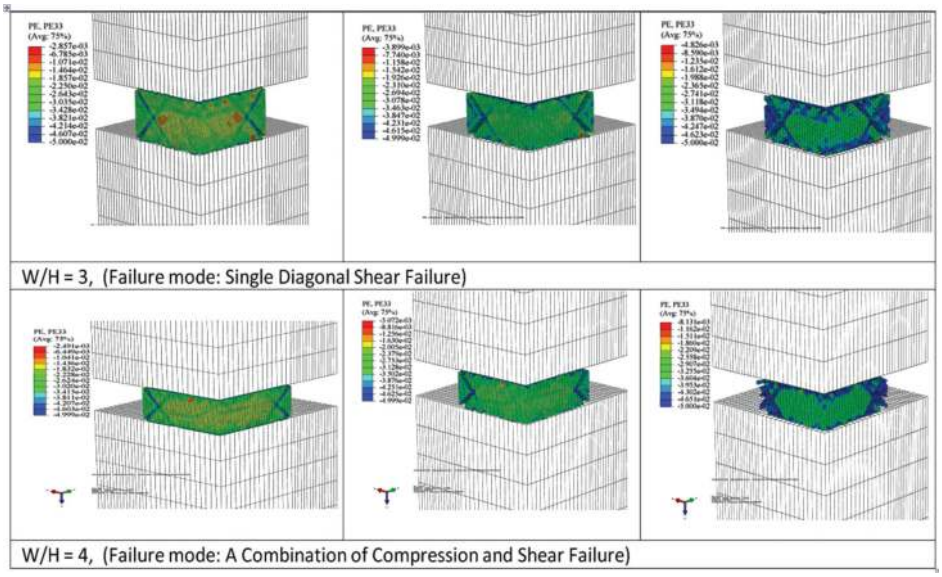

Figure 6. Failure mode of a single pillar with the different w/h ratios.

coal pillar model based on the symmetrical boundary conditions with respect to the different width by height (w/h) ratios of 1–10 were developed. It was observed that when the w/h ratios are less than 4, the failure mode of pillar can be either a double or a single diagonal shear failure in which the trajectory cracking starts from the edges and progresses towards the centre of the pillar. While the w/h ratios are greater than 4, the obtained possible failure mode would be a combination of the shear and compression failure modes. Thus, the trajectory of the cracking due to the pure compression failure would be propagated from the centre to the corners where a pillar gradually starts towards fully squashed (see **Figure 6**).

7. Remarkable conclusions

Analytical method is an important part of coal burst evaluation and forecasting. Analytical forecasting methods, either alone or combined with numerical simulations, can be used to estimate both *in situ* stress and induced stress, which leads to the prediction of failure-prone areas and calculation of critical values of the energies. The behaviour of a single pillar under different applied loads ranging from the quasi-static towards the dynamic loading conditions was simulated using commercial finite element package ABAQUS/Explicit. A strain-based failure condition was evaluated to determine the failure modes in a single pillar by respecting to the different w/h ratios. The observed numerical failure modes can be classified by shear and compression failures as well as a combination of both shear and compression were comprehensively illustrated. The released energy or residual energy is either transferred into kinetic energy or dissipated energy in non-elastic behaviour such as joint shear and fracturing. The unstable release of potential energy of the coal around the excavations, mainly in the form of kinetic energy, causes coal burst.

Author details

Faham Tahmasebinia*, Chengguo Zhang, Ismet Canbulat, Onur Vardar and Serkan Saydam

*Address all correspondence to: faham.tahmasebinia@sydney.edu.au

School of Mining Engineering, University of New South Wales, Sydney, Australia

References

[1] Linkov AM. Rockbursts and the instability of rock masses. International Journal of Rock Mechanics and Mining Sciences & Geomechanics Abstracts. 1996;**33**(7):727-732

[2] Gong QM, Yin LJ, SY W, Zhao J, Ting Y. Rock burst and slabbing failure and its influence on TBM excavation at headrace tunnels in Jinping II hydropower station. Engineering Geology. 2012;**124**(1):98-108

[3] Li S, Feng XT, Li Z, Chen B, Zhang C, Zhou H. *In situ* monitoring of rockburst nucleation and evolution in the deeply buried tunnels of Jinping II hydropower station. Engineering Geology. 2012;**137–138**:85-96

[4] Cai M. Principles of rock support in burst-prone ground. Tunnelling and Underground Space Technology. 2013;**36**:46-56

[5] Ortlepp WD, Stacey TR. Rockburst mechanisms in tunnels and shafts. Tunnelling and Underground Space Technology. 1994;**9**(1):59-65

[6] Tarasov BG, Randolph MF. Frictionless shear at great depth and other paradoxes of hard rocks. International Journal of Rock Mechanics and Mining Sciences. 2008;**45**(3):316-328

[7] Wang JA, Park HD. Comprehensive prediction of rockburst based on analysis of strain energy in rocks. Tunnelling and Underground Space Technology. 2001;**16**(1):49-57

[8] Cook NGW. Origin of rockbursts. In: Richards L, editor. Rockbursts; Prediction and Control. London: Institute of Mining and Metallurgy; 1983. pp. 1-9

[9] Wattimena RK, Sirait B, Widodo NP, Matsui K. Evaluation of rockburst potential in a cut-and-fill mine using energy balance. International Journal of the Japanese Committee for Rock Mechanics. 2012;**8**(1):19-23

[10] Mitri HS, Tang B, Simon R. FE modelling of mining-induced energy release and storage rates. The Journal of the South African Institute of Mining and Metallurgy. 1999;**99**(2):103-110

[11] Novozhilov VV. Foundations of the Nonlinear Theory of Elasticity. Graylock. Mineola, New York; 1999

[12] Ranzi G, Gilbert R. Structural Analysis: Principles, Methods and Modelling. Boca Raton. Florida: CRC Press; 2015

[13] Ranzi G, Dall Asta A, Ragni L, Zona A. A geometric nonlinear model for composite beams with partial interaction. Engineering Structures. 2010;**32**(5):1384-1396

[14] Xie HP, Li L, Peng R, Ju Y. Energy analysis and criteria for structural failure of rocks. Journal of Rock Mechanics and Geotechnical Engineering. 2009;**1**(1):11-12